Available online at www.sciencedirect.com
ScienceDirect
Journal of Molecular Catalysis A: Chemical 267 (2007) 112–119
JOURNAL OF MOLECULAR CATALYSIS A: CHEMICAL
www.elsevier.com/locate/molcata

# $H_2O$-controlled synthesis of $TiO_2$ with nanosized channel structure through *in situ* esterification and its application to photocatalytic oxidation

Song-Taek Oh [a], Jae-Suk Choi [a], Han-Su Lee [a], Lianhai Lu [a], Heock-Hoi Kwon [b], In Kyu Song [a], Jae Jeong Kim [a], Ho-In Lee [a,*]

[a] *School of Chemical and Biological Engineering and Research Center for Energy Conversion and Storage, Seoul National University, Seoul 151-744, Republic of Korea*
[b] *Department of Chemical and Environmental Engineering, Soongsil University, Seoul 156-743, Republic of Korea*

Received 13 November 2006; accepted 14 November 2006
Available online 21 November 2006

**Abstract**

$TiO_2$ with a characteristic nanosized channel structure was synthesized by the sol–gel reaction of a titanium precursor with water produced from the *in situ* esterification of acetic acid and polymers containing hydroxyl groups. Several polymers including polyethylene glycol, Pluronic P123, and Tween 20 were used in these reactions to optimize the resulting surface area and pore size. The prepared samples were characterized by X-ray diffraction, $N_2$ adsorption, thermogravimetric analysis, infrared spectroscopy, and field emission-scanning electron microscopy, and evaluated for photocatalytic decomposition of two hazardous compounds.

Contrary to the anisotropic structure of $TiO_2$ when prepared with considerable amounts of water, $TiO_2$ synthesized through *in situ* esterification had a relatively large and regular channel structure that originated from the inorganic–organic network that formed between template molecules and Ti species. This inorganic–organic network seemed to be induced by hydrolysis of the Ti precursor with the small amount of $H_2O$ produced from the esterification reaction. The effect of the type and quantity of polymer on the structural properties of the synthesized $TiO_2$ was also elucidated.

The relationship between the structural properties and the photocatalytic activities of the $TiO_2$ was investigated by studying the photodecomposition of probe materials with various molecular sizes. Photodecomposition of 2-isopropyl-6-methyl-4-pyrimidinol, a pyrimidine derivative, was limited by the $TiO_2$ channel size because its large molecular size restricted its diffusion into the $TiO_2$ channel. On the other hand, cyanide, with its relatively small molecular size, was effectively decomposed by $TiO_2$ photocatalysis, and the decomposition activity was proportional to the $TiO_2$ surface area regardless of the channel size.


*Keywords:* $TiO_2$; Photocatalysis; *In situ* esterification; Polyethylene glycol; 2-Isopropyl-6-methyl-4-pyrimidinol

## 1. Introduction

Heterogeneous photocatalysis has numerous advantages, including complete mineralization of harmful organic compounds and high degradation efficiency in removing organic pollutants even at ultra low concentrations. As a result, this process has attracted worldwide interests. Among various photocatalysts, $TiO_2$, with its versatile structure, has been studied extensively due to its high photocatalytic activity and its stability in various chemical and physicochemical environments [1–4].

The sol–gel method has been widely used to synthesize materials with various metastable structures even at relatively low temperatures since it provides excellent chemical homogeneity [5–7]. In this preparation method, it is possible to control the physical properties of the resulting materials including particle size, particle shape and pore structure by adjusting preparation variables. However, in the traditional sol–gel method for $TiO_2$ preparation, it is often difficult to control the rate of hydrolysis as titanium precursors are highly reactive toward water. As a result, the physicochemical properties of $TiO_2$ have been practically uncontrollable. Several attempts have been made to solve

* Corresponding author. Tel.: +82 2 880 7072; fax: +82 2 888 1604.
*E-mail address:* hilee@snu.ac.kr (H.-I. Lee).

1381-1169/$ – see front matter © 2006 Elsevier B.V. All rights reserved.
doi:10.1016/j.molcata.2006.11.028

this problem by addressing various aspects of the reaction conditions: adding strong acid or base to retard the reaction rate of both hydrolysis and condensation [8–11], and using polymers as templates to obstruct the contact between the titanium precursor and water molecules so that $TiO_2$ particles are induced to grow following the polymeric array in the solvent [12–18].

Recently, a novel $TiO_2$ preparation method was reported that involve *in situ* esterification of low molecular weight alcohols and acetic acid [19–23], where the water produced from the esterification was used for the hydrolysis reaction to produce size-controlled $TiO_2$ materials. Unfortunately, however, the physicochemical properties of prepared $TiO_2$, including surface area, pore size and photocatalytic activity, did not reach a satisfactory level due to the absence of template.

In the present study, a series of $TiO_2$ channel structures with various pore sizes and surface areas were synthesized through the *in situ* esterification of polymers that also served as bifunctional templates for supplying $H_2O$ and directing the structure. The resulting $TiO_2$ samples were evaluated for the photocatalytic decomposition of two harmful compounds with different molecular sizes: 2-isopropyl-6-methyl-4-pyrimidinol (IMP), a pyrimidine derivative, and cyanide ($CN^-$). After investigating the effects of the polymer templates on the structural properties and photocatalytic activities of the resulting $TiO_2$, several attempts were made to further increase the photocatalytic activity of $TiO_2$ for cyanide and IMP decomposition.

## 2. Experimental

### 2.1. Preparation of the $TiO_2$ catalysts

$TiO_2$ samples were synthesized by slowly dropping 0.02 mol of titanium tetraisopropoxide (TTIP, 98+%, Junsei) into excess anhydrous acetic acid (Merck) containing specified amounts of the polymer templates, polyethylene glycol (PEG, Aldrich), poly(ethylene-*co*-1,2-butylene)diol (PEB, Aldrich), Pluronic P123 (BASF), or Tween 20 (Aldrich). The solution was kept at 323 K overnight followed by hydrothermal treatment at 353 K for 4 days. The resulting white powders were then collected by filtration and subsequently washed with acetone. The collected powders were dried overnight in an oven at 383 K. Organic components in the dried powders were removed by heat treatment where the temperature was increased from room temperature to 773 K at a rate of 1 K/min and then kept at 773 K for 2 h.

### 2.2. Photocatalytic activity test

A cylindrical Pyrex photoreactor equipped with a stir bar was used in this study. The reactor temperature was maintained at 296 K with a water jacket. A high-pressure mercury lamp (Kum-Kang Co., $I_{max} \sim 360$ nm) was used as a UV light source. Deep UV light with wavelength shorter than 300 nm was cut off by a Pyrex window, and IR radiation from the UV light source was filtered out by the water jacket.

For the photocatalytic decomposition of IMP, 60 mg of $TiO_2$ was suspended in 300 mL of aqueous solution containing 24 mg of IMP. The concentration of IMP was monitored with a UV–vis spectrophotometer (UV-2401PC, Shimadzu) at the peak intensity of 253 nm to avoid the interference from the intermediate species that are ultimately decomposed to $CO_2$ by photocatalytic oxidation of $TiO_2$ [24]. For the photocatalytic decomposition of cyanide, 100 mg of $TiO_2$ was suspended in 300 mL of aqueous solution containing 24 mg of $CN^-$. After filtering the solution, the concentration of cyanide was determined by the standard silver nitrate titration method [25]. In each case, before conducting the activity test, the solution was thoroughly mixed and sonicated to exclude the dispersion effect of the catalysts.

### 2.3. Characterization

BET surface areas and pore size distributions of the prepared $TiO_2$ samples were determined by $N_2$-adsorption using an ASAP 2010 (Micromeritics) apparatus at 77 K. All samples were pretreated at 423 K under vacuum for 2 h. Pore size distributions were obtained from desorption isotherms using the Barrett–Joyner–Halenda (BJH) method. The powder X-ray diffraction (XRD) was measured on a Mac Science M18XHF$^{22}$-SRA diffraction spectrometer using Cu Kα as a radiation source. The average crystallite sizes of the prepared samples were estimated from the line broadening of the corresponding XRD peaks using the Scherrer equation. Thermogravimetric analysis (TGA) was conducted on a SDT Q600 (TA instruments). FT-IR experiments were performed on a Prospect IR spectroscope (MIDAC). The surface morphology of the prepared $TiO_2$ was studied with a field emission-scanning electron microscope (FE-SEM, JSM-6700F, JEOL).

## 3. Results and discussion

### 3.1. Preparation of $TiO_2$ with nanosized channel structure by in situ esterification

Table 1 summarizes the characteristics of the samples prepared by hydrolysis of TTIP with water produced from the *in situ* esterification of PEG and acetic acid; these samples are designated the TNE series ($TiO_2$ with nanosized channel structure prepared by esterification). PEG with a molecular weight of approximately 2000 was used for these experiments. The structural properties of the resulting $TiO_2$, such as surface area and pore size, were affected by the amount of PEG. Considering pore size and surface area, the optimum amount of PEG in the

Table 1
Characteristics of $TiO_2$ samples prepared through esterification of acetic with various amounts of PEG

| | Amount of PEG[a] (mmol) | Surface area ($m^2$/g) | Pore size[b] (nm) | Pore volume ($m^3$/g) |
|---|---|---|---|---|
| TNE-1 | 0.1 | 67 | 12.7 | 0.26 |
| TNE-2 | 0.2 | 68 | 18.7 | 0.30 |
| TNE-3 | 0.5 | 40 | 15.1 | 0.15 |
| TNE-4 | 1.0 | 17 | 3.9 | 0.05 |

[a] The molecular weight of PEG used was approximately 2000.
[b] Pore size was estimated at the peak point of the BJH pore size distribution plot obtained from the desorption branches of the isotherms.

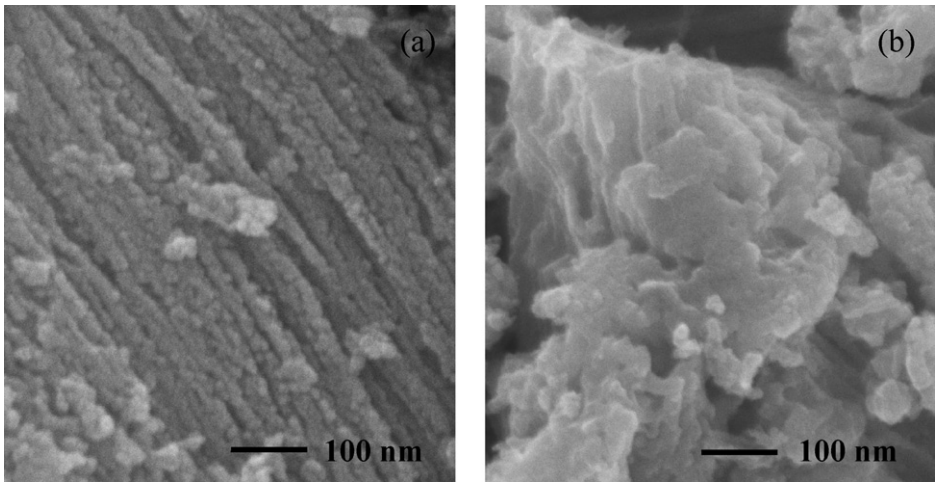


Fig. 1. FE-SEM images of $TiO_2$ samples prepared through *in situ* esterification of acetic acid with PEG of (a) 0.2 mmol (TNE-2) and (b) 1.0 mmol (TNE-4).

$TiO_2$ preparation was 0.2 mmol. TNE-2 had a large pore size of about 19 nm and relatively large pore volume. As seen clearly in the FE-SEM images in Fig. 1, TNE-2 had comparatively regular channel structure and the pore size was actually the inter-channel distance. On the contrary, pore collapses were observed in the TNE-4 sample due to agglomeration of $TiO_2$ particles. According to XRD patterns, the TNE series consisted of mainly anatase crystal structures mixed with a small amount of rutile structures (Fig. 2). The average anatase crystallite size of the TNE series was approximately 18 nm based on analysis of the characteristic XRD peak of (1 0 1) face at $2\theta = 25.55^\circ$ with the Scherrer equation. This size is in good agreement with the results of FE-SEM experiments.

In order to confirm the calcination temperature of 773 K, the TNE-2 sample was analyzed by a TGA experiment; the result is presented in Fig. 3. All organic compounds, including the template reagent, were completely removed from the $TiO_2$ sample when the temperature had reached or exceed 673 K. Considering all of the results given above, we propose that $TiO_2$ with a nanosized channel structure was successfully synthesized by *in situ* esterification using optimal amounts of PEG and acetic acid.

### 3.2. Role of water in the formation of nanosized channel structure

According to our previous report [19], when TTIP was added to a solution containing PEG, acetic acid and considerable amounts of water, the $TiO_2$ formed had anisotropic structure with low surface area and small pore size. This implies that the presence of large amounts of water limited the formation of the $TiO_2$ channel structure. In this case, esterification between PEG and acetic acid did not occur and TTIP was hydrolyzed by water without any interaction with PEG. In contrast, the small amount of water produced by *in situ* esterification seemed to interact via hydrogen bond with the hydrophilic oxygen of the PEG molecules and to subsequently hydrolyze TTIP to form a $TiO_2$–PEG network. The formation of this network is evidenced by FT-IR data of the dried $TiO_2$ samples as shown in Fig. 4. For the $TiO_2$ samples synthesized by *in situ* esterification without added water, typical peaks that originated from the acetate group esterified with PEG were observed at 1115, 1240 and

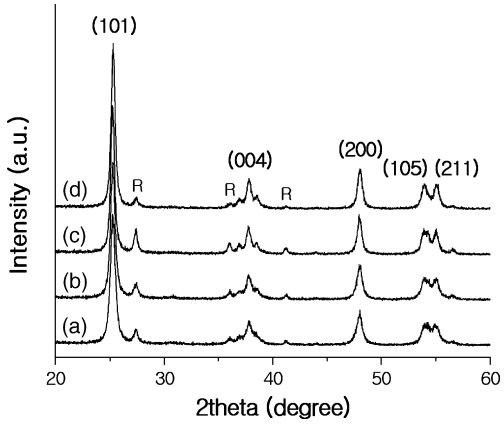


Fig. 2. XRD patterns of $TiO_2$ samples prepared through esterification of acetic acid with PEG of (a) 0.1 mmol (TNE-1); (b) 0.2 mmol (TNE-2); (c) 0.5 mmol (TNE-3); (d) 1.0 mmol (TNE-4).

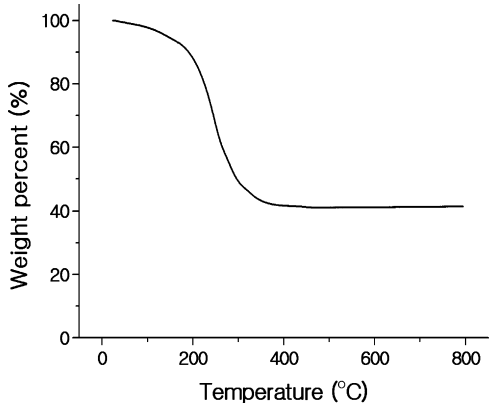


Fig. 3. TGA profile of $TiO_2$ sample prepared through esterification of acetic acid with PEG of 0.2 mmol (TNE-2).

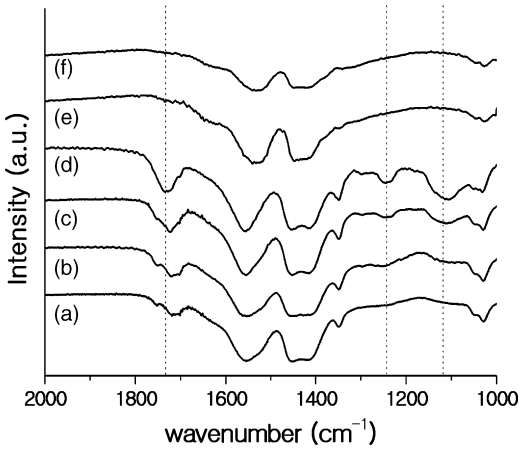


Fig. 4. IR spectra of dried $TiO_2$ samples prepared using PEG of (a) 0.1 mmol (TNE-1); (b) 0.2 mmol (TNE-2); (c) 0.5 mmol (TNE-3); (d) 1.0 mmol (TNE-4); (e) 0.2 mmol of PEG and water; (f) only water without PEG. The molar ratio of added water to TTIP was 200.

1730 $cm^{-1}$. The peaks were assigned after referencing the articles by Bu et al. [26]. The intensity of these peaks increased with increasing amounts of PEG, implying that the amount of PEG that participated in esterification also increased. However, these peaks did not appear in the $TiO_2$ samples synthesized in the presence of considerable amounts of added water (the molar ratio of $H_2O$ to TTIP was 200) although PEG and acetic acid were also present in the solution. This result is consistent with those reported previously, where researchers maintained that the formation of a regular pore structure with sufficiently large size was attributed to the organic–inorganic interaction between the template and $TiO_2$ that formed a crown-ether type network through weak coordination bonds [12,27].

In order to study the effect of the template structure on the structural properties of prepared $TiO_2$, PEB was used as structure-directing template instead of PEG. Fig. 5 illustrates the FE-SEM image of $TiO_2$ synthesized with PEB as the water-supplying template. The PEB has a similar molecular structure

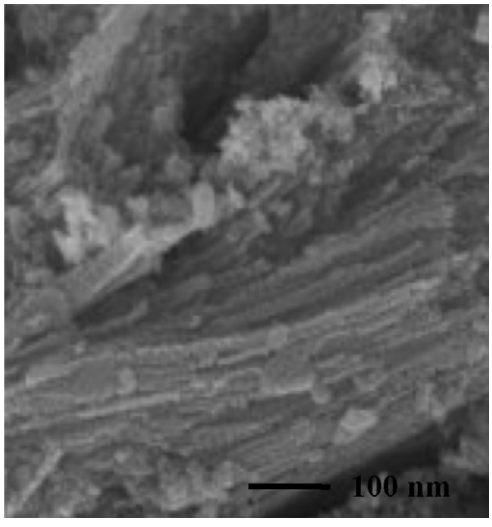


Fig. 5. FE-SEM image of $TiO_2$ sample prepared through esterification of acetic acid with PEB.

to PEG with hydroxyl groups on both ends, but lacks the hydrophilic ether oxygen present in the body of PEG. The PEB used had a molecular weight of approximately 2600. As seen in Fig. 5, the resulting channel structure was seriously distorted. We believe this is due to the structural characteristics of the PEB molecule. As with PEG, the presence of hydroxyl groups on both ends of the PEB molecule should allow the esterification of PEB and acetic acid to occur. However, because hydrophilic oxygen atoms are not present in the body of PEB, the water produced by the esterification could only interact with the carboxylic oxygen group produced by the esterification with acetic acid. Consequently, the $TiO_2$–PEB network was irregular and restrictive, and thus produced the distorted channel structure observed after calcination. Therefore, organic–inorganic interactions play a crucial role in the preparation of $TiO_2$ with a regular channel structure such that the *in situ* esterification method facilitated the formation of a regular organic–inorganic network by generating small amounts of $H_2O$ that in turn interacted with PEG molecules and hydrolyzed TTIP.

### 3.3. Relationship between structural properties and photocatalytic activity

In order to elucidate the effect of esterification time on the structural and photocatalytic properties of $TiO_2$, several samples were prepared by varying the esterification time, the amount of time that acetic acid and PEG were mixed before TTIP addition. The resulting $TiO_2$ samples were evaluated for photodecomposition of IMP and cyanide. Table 2 summarizes the structural properties and photocatalytic activities of these $TiO_2$ samples. The photocatalytic activities were described with $k$, the rate constant of the 1st order reaction. Even though all $TiO_2$ samples had similar specific surface areas (approximately 70 $m^2/g$), their pore sizes and pore volumes varied corresponding to the esterification time. The $TiO_2$ sample with the largest pore was obtained with 30 min of esterification. Other properties of the samples, such as crystal structures, UV–vis absorption properties, thermogravimetric characteristics, and surface organic functional groups, were virtually identical. As described in Table 2, the photocatalytic activities of these $TiO_2$ samples for IMP decomposition were affected by pore size. With a larger pore size, a higher 1st order reaction rate is achieved. We do not believe this occurs because of the differences in UV-light intensity with the larger pore since the activities for cyanide decomposition of these $TiO_2$ samples were almost the same regardless of the pore size. Rather, this indicates that the influence of pore size on IMP photodecomposition activity can be attributed to the differences in the diffusion rate of IMP molecules from the solution to the interior of the $TiO_2$ channel. Differences in IMP adsorption on the surface of $TiO_2$ samples can be excluded as we observed that there was almost no IMP adsorption on the prepared $TiO_2$ in an adsorption experiment without any UV illumination.

A similar relationship between the photocatalytic activity and the molecular size of the reactant was observed for $TiO_2$ samples prepared using PEG with varying molecular weight (named the TNG series, where the number following TNG indicates the molecular weight of the PEG used). Three channel-structured

Table 2
Structural properties and photocatalytic activities of several $TiO_2$ samples prepared with varying esterification time

| Esterification time[a] (min) | Surface area ($m^2$/g) | Pore size[b] (nm) | Pore volume ($m^3$/g) | $k_1$[c] ($\times 10^{-3}$ $min^{-1}$) | $k_2$[d] ($\times 10^{-3}$ $min^{-1}$) |
|---|---|---|---|---|---|
| 10 | 67 | 12.7 | 0.26 | 13.3 | 19.4 |
| 20 | 67 | 18.2 | 0.27 | 15.5 | 18.8 |
| 30 | 68 | 18.7 | 0.30 | 18.1 | 19.1 |
| 60 | 70 | 15.2 | 0.28 | 14.8 | 19.2 |
| 120 | 68 | 15.0 | 0.28 | 14.3 | 19.8 |
| P25[e] | – | – | – | 19.0 | 25.0 |

[a] The esterification time meant the mixing time of acetic acid and PEG before TTIP addition.
[b] Pore size was estimated at the peak point of the BJH pore size distribution plot obtained from the desorption branches of the isotherms.
[c] $k_1$ was the rate constant of the 1st order reaction for the photodecomposition of IMP.
[d] $k_2$ was the rate constant of the 1st order reaction for the photodecomposition of cyanide.
[e] P25 was selected for a reference photocatalyst.

$TiO_2$ samples that have different structural properties were synthesized with PEGs of three different molecular weights. The surface areas and pore sizes of the TNG series are shown in Fig. 6. A characteristic relationship between the structural properties of the prepared $TiO_2$ samples and the molecular weights of PEGs was observed such that, as the molecular weight of PEG increased, the specific surface area decreased while the average pore size increased. The photocatalytic activities of the TNG samples for IMP and cyanide decomposition are shown in Fig. 7. Among the samples in the TNG series, TNG200 and TNG2000 revealed the highest photocatalytic activity for cyanide and IMP decomposition, respectively. Moreover, the activities of TNG2000 for IMP decomposition and of TNG200 for cyanide decomposition were similar to those of P25 (listed in Table 2), a representative commercial photocatalyst for the same respective compounds. Considering the results shown in Figs. 6 and 7, it is clear that the photocatalytic activities of the prepared $TiO_2$ for decomposing IMP and cyanide were strongly related to the pore size and surface area of the catalysts. While the cyanide decomposition rate is directly proportional to the surface area of the $TiO_2$ sample, the IMP decomposition rate is somewhat complicated and relates to both the pore size and surface area. For better IMP decomposition, greater surface area coupled with appropriate pore size is necessary. We believe

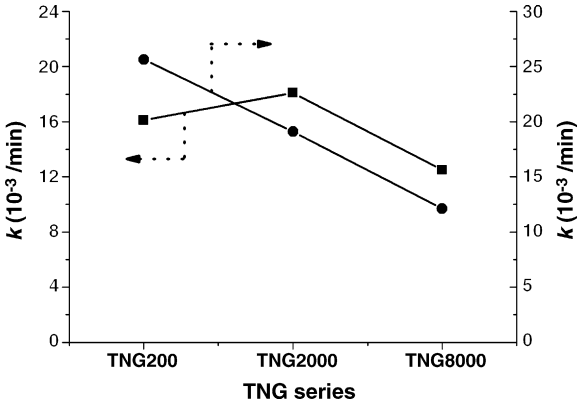


Fig. 7. Photocatalytic activity of $TiO_2$ prepared through esterification of acetic with varying molecular weight of PEG (named the TNG series). The solid squares and circles represent the activities of the prepared $TiO_2$ for IMP decomposition and for cyanide decomposition, respectively.

the difference in the molecular sizes of IMP and cyanide affect their ability to diffuse into the pore inside of the $TiO_2$ samples. Although the molecular sizes of IMP as well as cyanide were both smaller than the pore size of the prepared $TiO_2$, IMP has a bulkier molecular structure than cyanide, so that the pore size had a greater effect on its decomposition. Since the small

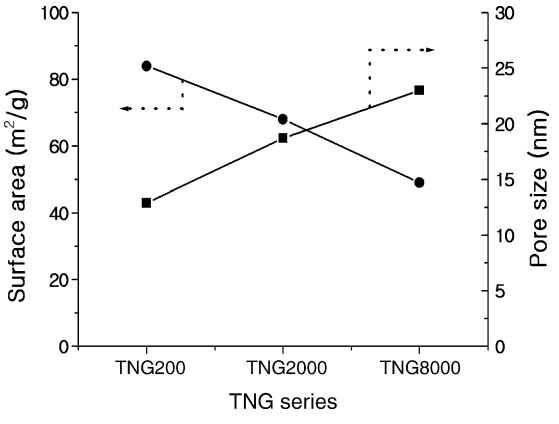


Fig. 6. Surface area and pore size of the $TiO_2$ samples prepared through esterification of acetic with varying molecular weight of PEG (named the TNG series). The solid circles and squares represent the surface area and pore size of the prepared $TiO_2$, respectively.

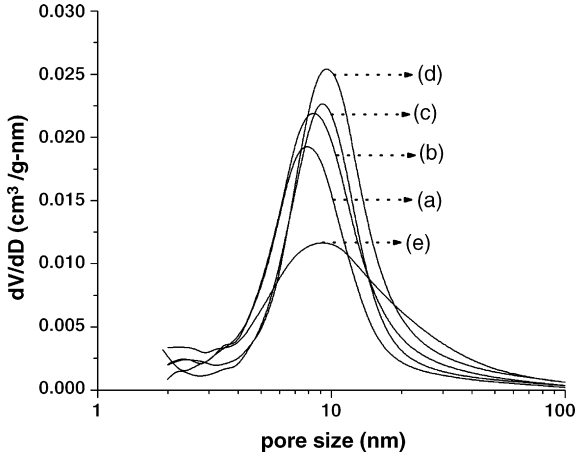


Fig. 8. Pore size distribution of the $TiO_2$ samples prepared through esterification of acetic with Pluronic P123 of (a) 0.125 mmol (TNP-1); (b) 0.25 mmol (TNP-2); (c) 0.5 mmol (TNP-3); (d) 1.0 mmol (TNP-4); (e) 2.0 mmol (TNP-5).

cyanide molecule relatively quickly and easily travels to the surface of $TiO_2$, the cyanide decomposition activity was proportional to the specific surface area of the catalyst regardless of the pore size. On the other hand, the relatively large IMP molecules are more difficult to transfer to the narrow channel inside. As a result, while TNG200 with its small pore size showed relatively low IMP decomposition photocatalytic activity in spite of its large surface area, TNG2000 displayed the best photocatalytic activity through its proper combination of pore size and surface area. For the TNG8000 sample, the poorly developed channel structure that originated from the larger template polymer molecules in the twisted state [27] caused the smaller surface area and resulted in the lower IMP decomposition photocatalytic activity even with its large pore size. In summary, by varying the molecular weight of the template reagent, we could manipulate the structural properties of $TiO_2$ and thus affect the activity of the photocatalyst.

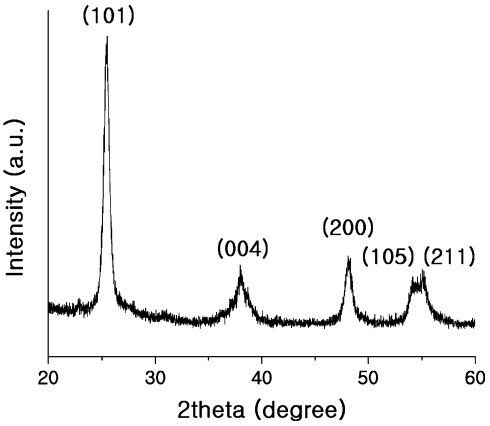


Fig. 9. XRD pattern of the $TiO_2$ sample prepared through esterification of acetic with Pluronic P123 of 1.0 mmol (TNP-4).

### *3.4. Preparation of highly active $TiO_2$ for the photodecomposition of cyanide and IMP*

In order to increase the photocatalytic activity of $TiO_2$ even further, we devised new routes to prepare catalyst samples with greater surface area to decompose cyanide and with larger pores to decompose IMP. $TiO_2$ samples with large surface areas were obtained using Pluronic P123 (molecular weight of approximately 5820) as the bifunctional template instead of PEG; these are designated the TNP series. Pluronic P123 has two hydroxyl groups at both ends, which can each produce $H_2O$ through ester-

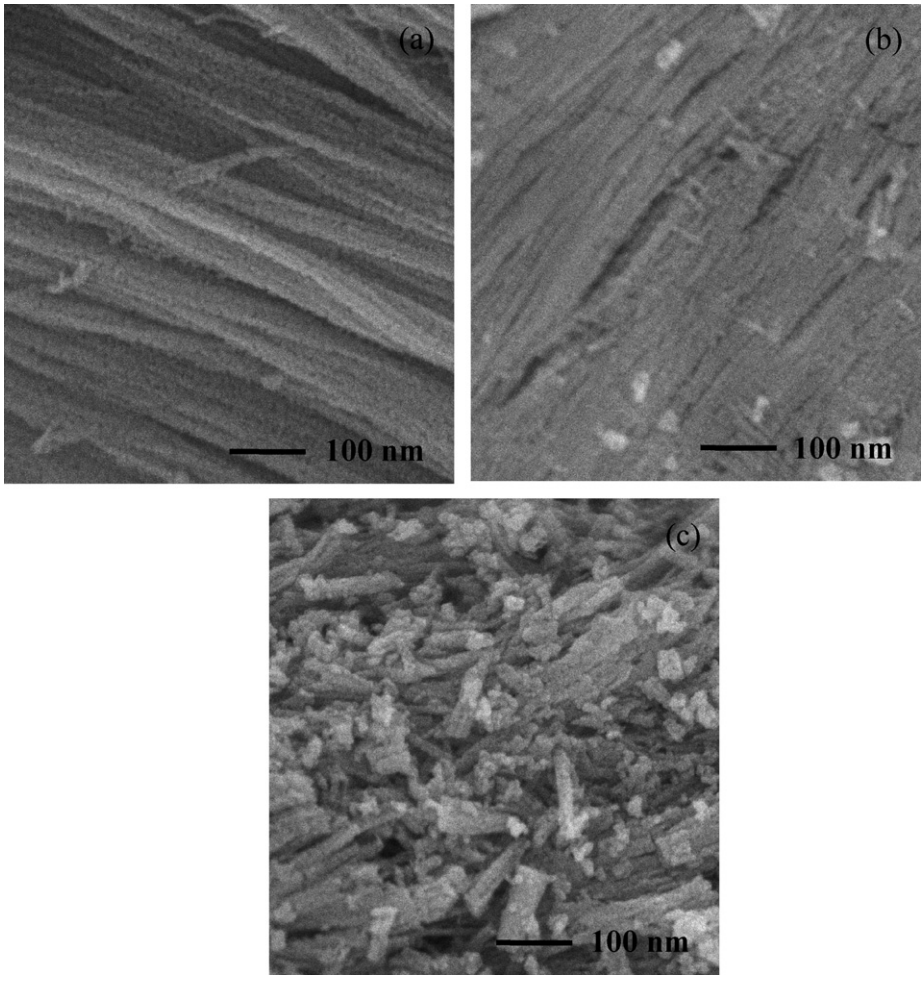


Fig. 10. FE-SEM images of $TiO_2$ samples prepared through esterification of acetic with Pluronic P123 of (a) 0.125 mmol (TNP-1); (b) 1.0 mmol (TNP-4); (c) 2.0 mmol (TNP-5).

Table 3
Structural properties and photocatalytic activities of $TiO_2$ samples prepared through esterification of acetic with Pluronic P123 (TNP series)

| TNP series | Amount of P123[a] (mmol) | Surface area ($m^2$/g) | Pore size[b] (nm) | Pore volume ($m^3$/g) | $k_1$[c] ($\times 10^{-3}$ $min^{-1}$) | $k_2$[d] ($\times 10^{-3}$ $min^{-1}$) |
|---|---|---|---|---|---|---|
| TNP-1 | 0.125 | 62 | 8.9 | 0.19 | 8.7 | 24.5 |
| TNP-2 | 0.25 | 71 | 8.9 | 0.23 | 9.0 | 27.2 |
| TNP-3 | 0.5 | 81 | 9.0 | 0.26 | 9.2 | 30.1 |
| TNP-4 | 1 | 94 | 8.8 | 0.31 | 9.4 | 36.7 |
| TNP-5 | 2 | 71 | 9.0 | 0.26 | 9.7 | 23.1 |

[a] The molecular weight of Pluronic P123 used was approximately 5820.
[b] Pore size was estimated at the peak point of the BJH pore size distribution plot obtained from the desorption branches of the isotherms.
[c] $k_1$ was the rate constant of the 1st order reaction for the photodecomposition of IMP.
[d] $k_2$ was the rate constant of the 1st order reaction for the photodecomposition of cyanide.

ification with acetic acid. Since this material is typically used as a surfactant, it was expected to form a stable $TiO_2$–polymer network in solution. As shown in Fig. 8, the pore size distributions of TNP series were relatively narrow with a pore size of about 9 nm, except of TNP-5. The crystal structure of TNP-4 was examined and turned out to be pure anatase phase (Fig. 9). The crystallite size of TNP-4 was about 13 nm, smaller than those of the TNG samples. The surface morphologies of some of the TNP series samples were examined with FE-SEM and are shown in Fig. 10. A regular but somewhat loose nanosized-channel was observed in the TNP-1 sample (Fig. 10(a)). Furthermore, the TNP-4 sample shown in Fig. 10(b) revealed a well-developed and close nanosized-channel, although some parts of the channel structures were twisted. On the other hand, a partially broken and less developed channel was observed in the TNP-5 sample, as shown in Fig. 10(c).

The structural properties and the photocatalytic activities of the TNP series for cyanide and IMP decomposition are summarized in Table 3. Rather than maintaining a constant pore size, the pore volumes and surface areas of the TNP series changed according to the amount of Pluronic P123; as the amount of Pluronic P123 increased, the surface areas and pore volumes of the corresponding samples increased and reached maximum values near 1.0 mmol of Pluronic P123. Interestingly, most TNP samples showed higher photodecomposition activity for cyanide than the commercially available P25, with the exception of TNP-5. The large surface area of TNP-4 allowed for a photocatalytic activity that was 40% greater than that of P25. However, TNP samples did not effectively decompose IMP due to their relatively small pore size and exhibited an activity nearly half that of P25.

In order to prepare $TiO_2$ with larger pores, Pluronic P123, Tween 20, with its bulky structure, and 1,3,5-trimethylbenzene (TMB) were used in combination. Although the pore size distribution of $TiO_2$ prepared with only Tween 20 was very broad in our preliminary experiments, Tween 20 used in conjunction with other polymers could contribute to the formation of large channels since the channel structure is formed in the space that the polymer occupied. TMB is known as a swelling agent that could increase the pore size by interacting with the hydrophobic propylene oxide in Pluronic P123 [28]. When these three polymers were combined, the resulting sample had a surface area of 75 $m^2$/g with a relatively broad pore size distribution (Fig. 11). As anticipated, its activity for IMP decomposition ($k$ was $22 \times 10^{-3}$ $min^{-1}$) was 20% greater than that of P25.

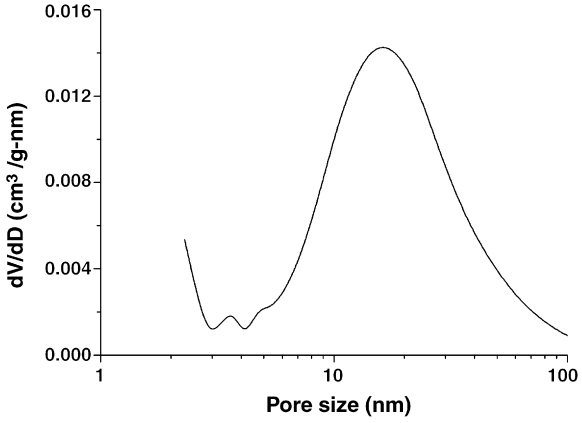


Fig. 11. Pore size distribution of $TiO_2$ sample prepared through esterification of acetic with Pluronic P123, Tween 20 and 1,3,5-trimethylbenzene (TMB).

## 4. Conclusions

$TiO_2$ samples with nanosized channel structure were successfully synthesized by the hydrolysis of titanium tetraisopropoxide with water produced from the *in situ* esterification of acetic acid and a polymeric template containing hydroxyl groups. The formation of channel structure in the prepared $TiO_2$ samples was analyzed by various methods including $N_2$ adsorption and scanning electron microscopy.

The polymers played a crucial role as bifunctional templates, both supplying the $H_2O$ necessary for hydrolysis and directing the resulting structure. *In situ* esterification of polymers with bulky structures seemed to be responsible for the formation of the nanosized channel that originated from the generation of an inorganic–organic network between template molecules and Ti species. Among the polymers employed, Pluronic P123 resulted in the greatest surface area of 94 $m^2$/g with a pore size of 9 nm, while a mixture of Pluronic P123, Tween 20 and 1,3,5-trimethylbenzene resulted in the largest pore size of 18 nm with a surface area of 75 $m^2$/g.

The prepared $TiO_2$ samples were evaluated in the photocatalytic decomposition of two probe materials with different molecular sizes: 2-isopropyl-6-methyl-4-pyrimidinol and cyanide. The activity for photodecomposition of the rela-

tively large 2-isopropyl-6-methyl-4-pyrimidinol was influenced by the channel size of $TiO_2$ due to its limited diffusion into the interior of the $TiO_2$ channel. On the other hand, the relatively small cyanide was decomposed well over the prepared $TiO_2$ samples; the activity was proportional to the surface area regardless of the channel size due to the ease of its transfer into the channel. Based on the 1st order reaction rate constant, the highest activities achieved for IMP and cyanide decomposition were 20% and 40% higher than those of P25, respectively.

## Acknowledgements

This work was financially supported by the Brain Korea 21 Program and by the ERC Program of MOST/KOSEF (Grant No. R11-2002-102-00000-0).

## References

[1] M.R. Hoffmann, S.T. Martin, W.Y. Choi, D.W. Bahnemann, Chem. Rev. 95 (1995) 69–96.
[2] M.R. Dhananjeyan, V. Kandavelu, R. Renganathan, J. Mol. Catal. A: Chem. 151 (2000) 217–223.
[3] H.-S. Lee, C.-S. Woo, B.-K. Yoon, S.-Y. Kim, S.-T. Oh, Y.-E. Sung, H.-I. Lee, Top. Catal. 35 (2005) 255–260.
[4] S.-S. Hong, C.-S. Ju, C.-G. Lim, B.-H. Ahn, K.-T. Lim, G.-D. Lee, J. Ind. Eng. Chem. 7 (2001) 99–104.
[5] R. Grieken, J. Aguado, M.J. Lopez-Munoz, J. Marugan, J. Photochem. Photobiol. A: Chem. 148 (2002) 315–322.
[6] A.J. Maira, K.L. Yeung, C.Y. Lee, P.L. Yue, C.K. Chan, J. Catal. 192 (2000) 185–196.
[7] D. Vorkapic, T. Matsoukas, J. Am. Ceram. Soc. 81 (1998) 2815–2820.
[8] H.-F. Yu, S.-M. Wang, J. Non-Cryst. Solids 261 (2000) 260–267.
[9] C.-C. Wang, J.Y. Ying, Chem. Mater. 11 (1999) 3113–3120.
[10] G. Pecchi, P. Reyes, P. Sanhueza, J. Villasenor, Chemosphere 43 (2001) 141–146.
[11] J. Yang, S. Mei, J.M.F. Ferreira, J. Am. Ceram. Soc. 83 (2000) 1361–1368.
[12] P. Yang, D. Zhao, D.I. Margolese, B.F. Chmelka, G.D. Stucky, Nature 396 (1998) 152–155;
P. Yang, D. Zhao, D.I. Margolese, B.F. Chmelka, G.D. Stucky, Chem. Mater. 11 (1999) 2813–2826.
[13] J.-Y. Zheng, J.-B. Pang, K.-Y. Qiu, Y. Wei, J. Mater. Chem. 11 (2001) 3367–3372.
[14] P.C.A. Alberius, K.L. Frindell, R.C. Hayward, E.J. Kramer, G.D. Stucky, B.F. Chmelka, Chem. Mater. 14 (2002) 3284–3294.
[15] X. Liu, J. Yang, L. Wang, X. Yang, L. Lu, X. Wang, Mater. Sci. Eng. 289 (2000) 241–245.
[16] K. Yoshinaga, M. Yamauchi, D. Maruyama, E. Mouri, T. Koyanagi, Chem. Lett. 34 (2005) 1094–1095.
[17] G.S. Devi, T. Hyodo, Y. Shimizu, M. Egashira, Sens. Actuators B, Chem. 87 (2002) 122–129.
[18] E.L. Crepaldi, G.J. de, A.A. Soler-Illia, D. Grosso, F. Cagnol, F. Ribot, C. Sanchez, J. Am. Chem. Soc. 125 (2003) 9770–9786.
[19] S.-T. Oh, L. Lu, H.-I. Lee, Mater. Lett. 60 (2006) 2795–2798.
[20] C. Wang, Z.-X. Deng, Y. Li, Inorg. Chem. 40 (2001) 5210–5214.
[21] N. Sijakovic-Vujicic, M. Gotic, S. Music, M. Invanda, S. Popovic, J. Sol–Gel Sci. Technol. 30 (2004) 5–19.
[22] J. Zhua, J. Zhanga, F. Chena, K. Iinob, M. Anpo, Top. Catal. 35 (2005) 261–268.
[23] W. Liu, A.-P. Chen, J.-P. Lin, Z.-M. Dai, W. Qiu, W. Liu, M.-Q. Zhu, S. Usuda, Chem. Lett. 33 (2004) 390–391.
[24] H.-S. Lee, T. Hur, S. Kim, J.-H. Kim, H.-I. Lee, Catal. Today 84 (2003) 173–180.
[25] J.-H. Kim, H.-I. Lee, Stud. Surf. Sci. Catal. 145 (2003) 161–164.
[26] S. Bu, Z. Jin, X. Liu, L. Yang, Z. Cheng, Mater. Chem. Phys. 88 (2004) 273–279.
[27] L. Zhang, Y. Zhu, Y. He, W. Li, H. Sun, Appl. Catal. B: Environ. 40 (2003) 287–292.
[28] D.Y. Zhao, Q.S. Huo, J.L. Feng, B.F. Chmelka, G.D. Stucky, J. Am. Chem. Soc. 120 (1998) 6024–6036.